Carbohydrate Polymer Technologies and Applications 11 (2025) 100875

Contents lists available at ScienceDirect

Carbohydrate Polymer Technologies and Applications

journal homepage: www.sciencedirect.com/journal/carbohydrate-polymer-technologies-and-applications

Development and characterization of novel tannin-modified konjac glucomannan hydrogels with optimized crosslinking features

Eleonora Verni [a,b], Francesca Sabatini [b,c], Chaehoon Lee [a,d], Giacomo Fiocco [a,e], Maduka Lankani Weththimuni [d], Barbara Vigani [f], Heiko Lange [b,c,g,*], Marco Malagodi [a,e,*], Francesca Volpi [a,e]

[a] Arvedi Laboratory of Non-Invasive Diagnostics, CISRiC, University of Pavia, 26100 Cremona, Italy
[b] Department of Earth and Environmental Sciences, University of Milano-Bicocca, 20126 Milan, Italy
[c] NBFC – National Biodiversity Future Center, 90133 Palermo Italy
[d] Department of Chemistry, University of Pavia, 27100 Pavia, Italy
[e] Department of Musicology and Cultural Heritage, University of Pavia, 26100 Cremona, Italy
[f] Department of Drug Sciences, University of Pavia, 27100 Pavia, Italy
[g] Biochemical Process Engineering, Division of Chemical Engineering, Department of Civil, Environmental and Natural Resources Engineering, Luleå University of Technology, SE-971 87 Luleå, Sweden

ARTICLE INFO

Keywords:
Konjac
Hydrogels
Polyphenols
Boric acid
Mechanical properties
Water retention
Cleaning

ABSTRACT

Konjac glucomannan (**KGM**) is a non-toxic, biodegradable polysaccharide known for its excellent gel-forming properties and high water retention. This study presents a novel tannin-enhanced **KGM** hydrogel, tailored for controlled solvent release and improved surface adaptability in artwork cleaning applications. Hydrogel formulation consisting of **KGM** crosslinked with borax was optimized generating borax through the reaction of boric acid and sodium hydroxide. This resulted in uniformly crosslinked gels with improved tensile strength and high moisture retention, essential for controlled cleaning. Moreover, tannins were incorporated in the optimised **KGM**-based polymer matrices. This modification was introduced as a novel and sustainable strategy to enhance crosslinking, leveraging natural polyphenols to add functional properties. Two tannins were tested: a condensed tannin isolated from *Vitis vinifera*, and a hydrolyzable tannin isolated from oak, tannic acid. Tannins were incorporated either through hydrogen bonding or covalently. Covalent attachment was achieved using epichlorohydrin (**ECH**) to add an epoxide motif to the tannin, enabling covalent binding with **KGM**. The resulting gels were thoroughly characterized for their chemical, rheological and morphological properties, showing that novel crosslinking *via in situ* borax formation improved moisture retention and surface adaptability, while the incorporation of tannins enhanced water absorption, maintaining high retention and favorable mechanical properties.

1. Introduction

Glucomannans are polycarbohydrates present in various natural sources like tubers, bulbs and roots, as well as both hardwoods and softwoods (Spiridon & Popa, 2008). Among those, the best-known raw material for glucomannan production is konjac (*Amorphophallus konjac*), given its high glucomannan content and the facile extraction of the polycarbohydrate (Gómez et al., 2017; Srzednicki & Borompichaichartkul, 2020). Konjac glucomannan (**KGM**) is a high molecular weight, non-ionic polysaccharide, consisting of d-mannose and d-glucose linked by β(1→4) bonds. It contains a low amount of acetyl groups, present at the C-3 position of the mannose units, that facilitate water solubility at low concentrations (Davé & McCarthy, 1997). Due to its excellent biocompatibility, non-toxicity, biodegradability and high content of hydroxyl groups, **KGM** has been applied in multiple fields including food industry, where it serves as a thickener, gelling agent and stabilizer, (Halim et al., 2023; Zhang et al., 2022), in biomedical fields like wound dressing, (Luan et al., 2017; Zhou et al., 2022) and in cosmetics and skin care products due to their moisture-retaining ability (Ervina et al., 2020; Paufique, 2010).

* Corresponding authors.
E-mail addresses: heiko.lange@ltu.se, heiko.lange@unimib.it (H. Lange), marco.malagodi@unipv.it (M. Malagodi).

https://doi.org/10.1016/j.carpta.2025.100875
Received 12 March 2025; Received in revised form 31 May 2025; Accepted 31 May 2025
Available online 2 June 2025

The most common crosslinking method to form **KGM** hydrogel is alkali-induced gelation, widely applied in food technology and biomedical engineering (Lee et al., 2022; Z. Liu et al., 2021; Zhang et al., 2022). Another crosslinking method involves the use of sodium tetraborate decahydrate ($Na_2B_4O_7{\bullet}10H_2O$, *i.e.*, borax). The hydrogel forms *via* interchain crosslinking of two *cis*-diol pairs from **KGM**, mediated by borate ions (Gao et al., 2008). These hydrogels are transparent, capable of self-healing, pH-responsive and of flexible texture, as intermolecular bonding involving borax and konjac motifs is reversible (Chen et al., 2019; Song et al., 2019). These characteristics render **KGM**-borax hydrogels well-suited for biomedical applications such as wound healing, (Song et al., 2019; Zhou et al., 2022) as well as for wastewater treatment, where their adsorption capacity enables the removal of dyes and heavy metals (Oishi & Maehata, 2013). Recently, **KGM**-borax hydrogels were applied to provide water and other solvents in very low amounts in the cleaning of water-sensitive surfaces such as historical wooden musical instruments, highlighting their advantageous moisture properties, texture and cleaning efficacy in the cultural heritage field (Chelazzi et al., 2020; Lee et al., 2022). In this field, cleaning procedures should ensure the safe removal of superficial contaminants such as dust, soil, grease, etc., without affecting the underneath layer (Fiocco et al., 2021; Lee et al., 2024a). For an effective and safe application, hydrogels must exhibit chemical inertness and optimal moisture management, meaning they should absorb a substantial amount of solvent while also regulating its release effectively. They must be resistant to breakage to prevent leaving residues, and sufficiently flexible to adapt to uneven surfaces (Borysenko, 2021; Sansonetti et al., 2020). Additionally, hydrogels should ideally be transparent or whitish to enable visual monitoring of cleaning events, to assess cleaning efficacy eventually by means of spectroscopic methods, and to ensure precision to the conservator (Micheli et al., 2014).

The gelling mechanism for hydrogels formed with borax as a crosslinking additive, such as the previously reported **KGM**-borax gel (Lee et al., 2022), is based on the dissociation of borax in an aqueous medium, resulting in an equilibrium involving boric acid ($B(OH)_3$), borate anions ($[B(OH)_4]^-$), and sodium cations (Na^+). However, the solubility of borax in water is known to be low, *i.e.,* 31.7 g/L (John & Colin D., 2013) and it is also reported that the borax-containing hydrogels often suffer from an inhomogeneous structure caused by insufficient mixing of the borax with the polymer matrix (Figure S1) (Chmara, 2024). A smooth structure is more desirable since it would guarantee a more uniform interaction, or action on and with the surfaces to be cleaned, and thus a more evenly distributed cleaning effect. This is especially the case when the cleaning is not supposed to be done with swiping movements, but in a stationary fashion, placing slabs of hydrogel on the surface. To sustainably enhance **KGM**-borax hydrogel properties, *i.e.*, microstructure, hydrophilicity, moisture retention, and tensile strength, natural polyphenols can be incorporated as structurally diversifying, essentially more flexible and thus more random elements that actively participate in the crosslinking.

Natural polyphenols are secondary metabolites derived from the pentose phosphate, shikimate, and phenylpropanoid pathways in plants, and exist in form of lignins, lignans, and tannins (Randhir et al., 2004). Tannins exist in a threefold structural variety. Gallotannins and ellagitanninsare soluble and cleavable into their components in hot water or in the presence of a tannin-specific enzyme, *e.g.*, tannase, and are thus termed 'hydrolysable' tannins. Tannin species without carbohydrate moieties, termed proanthocyanidins, polyflavonoid tannins, catechol-type tannins or pyrocatecollic type tannins, are stable under these conditions and thus called 'non- hydrolysable' or 'condensed' tannins (Haslam, 1989; Khanbabaee & Ree, 2001; Pizzi, 2008). An example for condensed tannins, which are derived from the flavonoid pathway, are the tannins obtained from wine, *i.e., Vitis vinefera* (***Vv***), consisting normally in a mix of procyanidins and profisetidins (Fig. 1a) (Zhen et al., 2021b). These have relatively small structures with a high phenol group content. An example for a hydrolysable tannin, derived from the shikimate pathway, is tannic acid (**TA**), isolated from oak galls or from oak bark, presenting a more voluminous structure and still higher phenolic content (Fig. 1b). Most notably, like glucomannan, tannins can also be obtained from waste biomass, *i.e.*, from the residues of the wine, forestry, wood and furniture industries. Tannins have gained increasing interest due to their antioxidant and antimicrobial properties,(Fraga-Corral et al., 2021; Giannì et al., 2020; Koleckar et al., 2008; Villanueva et al., 2023) and UV protection capabilities,(Alfonsi et al., 2023; Liao et al., 2019) and they have been explored as valuable biomaterial mediators or bioactive additives in various tissue engineering applications (Buzzini et al., 2008; Kim et al., 2020; Pizzi, 2008; Wei et al., 2023). The antioxidant, radical scavenging, and antimicrobial properties of tannins can also been useful in the context of the cleaning of cultural heritage items, where they might contrast, for example, the oxidative damage of sensitive surfaces eventually provoked by an additional or previously used cleaning agent that left residues. Their biological activity can be exploited to lower the number of bacteria on the surface of cultural heritage objects that could thrive on some of the historic organic coatings and thus destroy the objects.

Chemically, tannins exhibit versatile crosslinking capabilities in the context of hydrogels through various potential binding mechanisms, including hydrophobic coordination, electrostatic interaction, hydrogen and ionic bonding; consequently, numerous studies have investigated polyphenols as crosslinking agents, being able to add interesting features to hydrogel matrices (Alavarse et al., 2022; Jafari et al., 2022; Shavandi et al., 2018; Tang et al., 2025, 2024).

Apart from structurally diversifying the hydrogel matrix, this study aims to develop novel KGM-based hydrogel formulations displaying a much more uniform crosslinker incorporation, for ultimately improving both mechanical and moisture properties, using a sustainable approach suitable for cleaning cultural heritage surfaces.

To achieve the desired characteristics, the preparation of the newly developed KGM-based hydrogels was devised in three approaches. The first focuses on the facilitation of uniform crosslinking and generation of a homogeneous, particle-free matrix, which was hypothesized to happen by incorporating boric acid (H_3BO_3) (**BA**) and sodium hydroxide (NaOH) for an *in situ* generation of borax. **BA** can overcome the low solubility problem of borax, granting consistent incorporation of the crosslinking agent across the whole volume of water.

As a second way of varying hydrogel characteristics, ***Vv*** and **TA** tannins were added to sustainably advance the crosslinking system by offering non-linear structures capable of a more flexible crosslinking and, thus, a means to manipulate pore sizes within the hydrogel structures.

In a third approach, incorporation of tannins and *in situ* borax formation was accompanied by the addition of epichlorohydrin (**ECH**) as a second, organic crosslinker, diversifying chemical bonding between **KGM** and tannins, moderating the strong hydrophilicity introduced by the boron-based crosslinker. E**ECH**, was selected for beeing a commonly used, biobased crosslinker known for its ability to react with hydroxyl and phenolic groups, forming stable covalent networks (Kuniak & Marchessault, 1972; Nouailhas et al., 2011; Obaid et al., 2025). Its compatibility with both polysaccharides and polyphenols makes it particularly suitable for the dual-network design proposed in this study. Moreover, **ECH** is obtainable from renewable resources, (Bell et al., 2008) aligning with the sustainable strategy of this work.

Typically, polyphenols undergo pre-functionalization with **ECH**, with the resulting epoxidized polyphenols serving as starting material for the synthesis of new substances (Ferruti et al., 2023; Vera & Urbano, 2021).

In this study, a novel one-step process is presented for combining the synthesis with tannin-enhanced konjac glucomannan hydrogels with optimised, *in situ*-realised crosslinking with different crosslinking systems, both singularly or in combination, for generating hydrogels with improved mechanical features.

The realised gels were comprehensively characterized in terms of

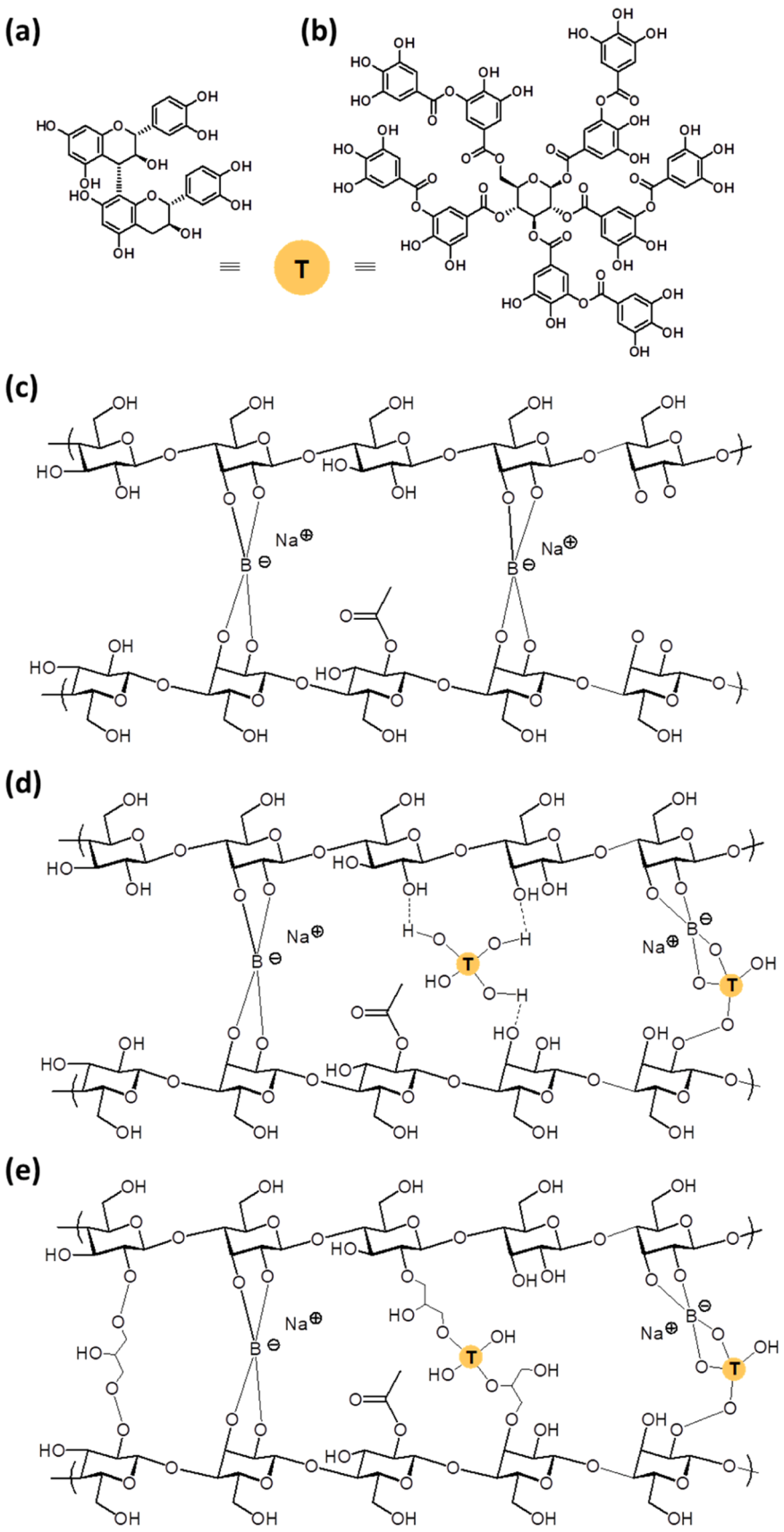

Fig. 1. Chemical structures of *Vitis vinifera* tannin (***Vv***) (a), tannic acid (**TA**) (b) and a conceptual structural representation of the various crosslinking means applied in this work, *i.e., in situ* borax-based (c), using tannins and *in situ* borax (d), and using tannins together with epichlorohydrin (**ECH**) and *in situ* borax (e).

their morphology and chemical composition through microscopy and spectroscopic analyses. Additionally, the moisture content, thermal and mechanical characteristics of the new gels were measured to identify promising products for the cleaning of cultural heritage artefacts. The various data are further compared to a reference system consisting in a borax-crosslinked **KGM** hydrogel previously reported (Lee et al., 2023).

2. Materials and methods

2.1. General information

The purified konjac glucomannan (**KGM**) (≥ 95 % pure, molecular weight of ~200.000 g/mol) was acquired from Hubei Yizhi Konjac Co. Ltd (Yichang, China) and used without further purification. High-purity water Milli-Q from Millipore Corporation (Merck KGaA, Darmstadt, Germany) was used for all the procedures. Sodium tetraborate decahydrate ($Na_2B_4O_7 \bullet 10H_2O$, borax) was purchased from Carlo ERBA (Cornaredo, Italy) and boric acid (H_3BO_3, **BA**) from Fluka (Morris Plains, New Jersey, USA). *Vitis vinifera* tannin (***Vv***) and tannic acid (**TA**) were isolated from waste biomass in form of wine and oak tree pruning residues (wood components of *Quercus robur*), and analysed for structural aspects using procedures established earlier (Zhen et al., 2021a). Epichlorohydrin (**ECH**), 2,2-diphenyl-1-picrylhydrazyl (**DPPH**), and methanol (HPLC grade) were purchased from Sigma-Aldrich (Merck KGaA, Darmstadt, Germany). The process of production of the reference system, *i.e.*, borax-crosslinked **KGM**-based hydrogel (**K_borax**) was performed as described earlier (Lee et al., 2023).

2.2. Preparation of KGM-based hydrogel with in situ formation of the borax crosslinker (K_BA)

For preparing KGM-based hydrogels with *in situ* borax formation (**K_BA**), **KGM** and **BA** were mixed in a ratio of 2:1 (m/m) and were suspended at a concentration of 3 % (m/v) in a solution of ethanol in Milli-Q water (5 % v/v). The suspension was kept stirring for approx. 30 s. Afterwards, 1 M aqueous solution of NaOH was added at a molar ratio of 1:15 relative to the stoichiometric amount required for complete reaction with **BA**. The gel was transferred to a falcon tube and left in a water bath at 50 °C for 45 min to stabilize and homogenize the hydrogel. The hydrogel was stored at 4 °C until use.

The amounts of each product used for the preparation of these hydrogels are listed in Table 1.

2.3. Preparation of tannin-modified KGM-based hydrogel with in situ formation of the borax crosslinker (K_BA_V and K_BA_T)

The preparation of KGM-based hydrogels modified with tannins (**K_BA_V** and **K_BA_T**) was carried out in analogy to the synthesis of the **K_BA** sample described in Section 2.2. The weight ratio of **KGM** over tannin, either ***Vv*** or **TA**, was fixed to 95:5 (m/m). Firstly, the tannin was dispersed in the mixture of ethanol and Milli-Q water at a concentration of 0.1 % (m/v), and the suspension was sonicated for 10 min to achieve complete dissolution. Afterwards, **KGM** and **BA** were added to the tannin solution in concentrations of 2 % (m/v) and 1 % (m/v), respectively. Then, 1 M aqueous solution of NaOH was added at a molar ratio of 1:15 relative to the stoichiometric amount required for complete reaction with **BA**, considering also the amount of NaOH consumed by the phenolic groups of the tannins, which were determined as described before (Zhen et al., 2021a). The mixture was then stabilized as described in Section 2.2. The hydrogels were stored at 4 °C until use.

Table 1
Composition of the formulated KGM-based hydrogels. The amounts of konjac glucomannan (**KGM**), boric acid (**BA**), polyphenol (**PP**), *i.e.*, either **Vv** or **TA**, milliQ water (H_2O), ethanol (EtOH), sodium hydroxide (NaOH), and epichlorohydrin (**ECH**) are reported.

Name	KGM [g]	BA [g]	PP [g]	H_2O [mL]	EtOH [mL]	NaOH [mL]	ECH [mL]
K_borax	1.20	0.60	—	57.00	3.00	—	—
K_BA	1.20	0.60	—	55.12	2.90	1.98	—
K_BA_V	1.14	0.60	***Vv***, 0.06	55.12	2.90	1.98	—
K_BA_V-E	1.14	0.60	***Vv***, 0.06	54.34	2.86	2.25	0.55
K_BA_T	1.14	0.60	**TA**, 0.06	55.12	2.90	1.98	—
K_BA_T-E	1.14	0.60	**TA**, 0.06	53.84	2.83	2.43	0.90

2.4. Preparation of tannin-modified KGM-based hydrogel with ECH as crosslinker (K_BA_V-E and K_BA_T-E)

The gel was prepared using the methodology outlined in Section 2.3, with the modification that, following the dispersion of tannin in a mixture of ethanol and Milli-Q water, **ECH** was stoichiometrically added relative to the phenolic OH content of each tannin. Eventually, the gel was left in a water bath at 60 °C for 45 min to ensure complete reaction of the **ECH** and stabilize the gel. The hydrogels were stored at 4 °C until use.

2.5. ATR-FTIR spectroscopy

Chemical characterization of the gel was performed by Fourier-Transform Infrared spectroscopy in Attenuated Total Reflection mode (ATR-FT-IR). Spectra were acquired with a Nicolet iS10 spectrometer (Thermo Fisher Scientific, Waltham, MA, USA) equipped with an iTR Smart device (total scan 32, range 4000 - 800 cm^{-1}, resolution 2 cm^{-1}).

2.6. UV–Vis spectroscopy

For UV–Vis spectroscopy analysis, tannin-containing hydrogels were dispersed in water with the aid of an Ultra-Turrax homogenizer (T-25 basic, Janke and Kunkel IKA, Germany), to yield a final tannin concentration of 10 ppm. The pH was adjusted to approximately 8, and the samples were subsequently analyzed with a Jasco V-730 UV–Vis spectrometer (Jasco Inc., Easton, US) (scan speed 8000 nm/min, range 250 - 400 nm, resolution 1 nm). Spectra were subsequently normalized to their maximum absorbance.

2.7. Scanning electron microscopy (SEM) imaging

Samples of the various gels were freeze-dried and metalized using a gold coating. At least 5 images for each gel in different sample regions were acquired. Measurements were carried out on a Tescan MIRA 3XMU series field emission FE-SEM microscope (TESCAN, Brno, Czech Republic) with an accelerating voltage of 5 kV in a high vacuum.

2.8. Color and opacity measurements

A portable Konica Minolta CM-2600d spectrophotometer (Chiyoda, Tokyo, Japan) was employed for colorimetric measurements. The average of the specular component included (SCE) values of 5 repetitions for each sample was considered and the dataset was processed in the CIE 1976 L*a*b* space. The opacity of the samples was calculated by means of their contrast ratio, which is the ratio of the reflectance of a hydrogel (5.00 ± 0.05 mm thick) when backed by a black standard to that when backed by a white standard of a known reflectance (Inokoshi et al., 1996). The contrast ratio (CR) is defined as $CR = Y_b/Y_w$ where Y_b is the tristimulus value Y of the sample on the black background and Y_w is the tristimulus value Y of the sample on the white background. The results are presented as percentages.

2.9. Determination of antioxidants by the DPPH radical scavenging activity

Adapting established protocols (Szabo et al., 2007), a stock solution for each freeze-dried hydrogel was prepared at a concentration of 0.2 mg/mL in aqueous methanol (40 % (v/v)). A **DPPH** stock solution was prepared by dissolving 50 mg of **DPPH** in 10 mL of aqueous methanol (40 % (v/v)). Using a 96 well plate, each sample was analyzed using a series of five concentrations, *i.e.*, 200, 160, 120, 80, and 40 μg/mL against a blank sample, employing for each measurement 100 μL of the **DPPH** stock solution. Aqueous methanol (40 % (v/v)) was used to adjust volumes as needed to arrive at a final volume of 125 μL in each well. All mixtures were incubated for 30 min in the dark before spectrophotometric analysis at λ = 519 nm using a Biochrom ASYS UVM340 plate reader (Biochrom, Waterbeach Cambridge, UK).

2.10. Determination of moisture properties

Moisture properties were obtained following a procedure described elsewhere (Domingues et al., 2014; Ming Kuo et al., 1999). In short, hydrogels were sliced into 1 × 1 × 0.2 cm blocks and dried overnight; afterwards, each gel was soaked for 5 h obtaining a fully swollen state gel. The equilibrium water content (EWC) and the swelling capacity (SC) were calculated as follows:

$$EWC(\%) = \frac{(W_w - W_d)}{W_w} \times 100$$

$$SC(\%) = \frac{(W_w - W_d)}{W_d} \times 100$$

where W_d is the initial weight of the dried gel and W_w is the weight of the gel after it absorbed water.

The soaked gels were placed on filter paper (Advantec MFS, Inc., 55 mm) for 30 min. The filter paper was weighed before and after the application of the gel to assess the retention capability (RC), calculated as follows:

$$RC\left(\frac{mg}{cm^2}\right) = \frac{(F_w - F_d)}{Area}$$

where F_d is the initial weight of the filter paper, and F_w is the weight of the filter paper with the moisture released from the gel.

To further understand the correlation between water uptake (WU) and water release (WR), the values of WR/WU were calculated as follows: (Lee et al. 2024b)

$$WR \Big/ WU(\%) = \frac{(F_w - F_d)}{(W_w - W_d)} \times 100$$

2.11. Thermogravimetric analysis

Thermogravimetric analysis (TGA) was performed using a thermobalance TGA 2 (Mettler Toledo, Nänikon, Switzerland). Typical sample amounts of around 5 mg were weighed in oven-dried 70 μL ceramic pans. Exact sample weights were determined automatically using the inbuilt balance of the calorimeter. TGA measurements were carried out at a heating rate of 10 °C/min from 25 to 1100 °C under nitrogen flow (50 mL/min). Experiments were run in triplicate. STARe software version 18.00 was used for data acquisition. TGA graphs were collected, showing typical mass loss with regards to temperature and related derivative (DTG) graphs were generated, showing mass loss rate *versus* temperature. The thermal parameters were determined by fitting the DTG curves using Origin software.

2.12. Differential scanning calorimetry

Differential scanning calorimetry (DSC) was performed using a Mettler Toledo DSC 3 Calorimeter (Mettler Toledo, Nänikon, Switzerland). Typical sample amounts of around 5 mg were exactly weighted in 40 μL aluminum pans, which were closed with a lid that was centrally punctured to prevent pressure built-up. An empty pan was used as a reference. DSC experiments were carried out under nitrogen flow (50 mL/min), temperature was scanned by a double heating-cooling cycle from 20 °C to 400 °C with a heating rate of 10 °C/min and a cooling rate of 25 °C/min. Experiments were run in triplicate. STARe software version 18.00 was used for data acquisition and Origin software for data visualization.

2.13. Determination of mechanical properties

Gel mechanical properties were assessed by means of a TA.XT Plus Texture Analyzer (Stable Micro Systems, Godalming, United Kingdom), equipped with a 5 kg load cell, both in tensile and compressive modes.

Before the tensile test, the hydrogels were first sliced into 2 mm-thick sections and then cut into rectangular specimens (3 × 1 cm) with the aid of a custom-made template to maintain consistent geometry across samples. Specimens were clamped onto an A/TG tensile grips probe, setting an initial distance of 1 cm between the grips. Sample thickness was measured using a Sicutool 3955G-50 (Sicutool, Milan, Italy) device prior to tensile testing. The analysis was conducted following a procedure described elsewhere (Said & Sarbon, 2022; Vigani et al., 2022). The upper grip raised at a constant speed of 2 mm/min for a distance of 50 mm. The tensile strength and the elongation % were calculated for each sample. Five replicates were performed.

Moreover, gel hardness was investigated through a compressive test. Samples were prepared in cylindrical molds with dimensions of 30 mm in diameter and 30 mm in height. A TA.XT plus Texture Analyzer, equipped with a P/10 measuring system consisting of a cylindrical probe with a diameter of 10 mm, was used to apply uniaxial forces perpendicular to the sample surface (Hurler et al., 2012). The probe was lowered with a test speed equal to 10.0 mm/s in order to determine a 70 % sample deformation. Hardness, that is the maximum compressive force per unit area required for sample destructuring, was calculated. Five replicates were performed.

3. Results and discussion

3.1. Hydrogel formation and characterization of their chemical, structural and morphological properties

A series of six hydrogels were prepared based on **KGM** as the main matrix element (Table 1), to compare their characteristics against the current standard, *i.e.*, borax-crosslinked KGM-based hydrogel **K_borax** that has been reported before.(Lee et al., 2023)

The chemical composition of the hydrogels and consequently their relative structure was characterized using ATR-FTIR spectroscopy, and the various observed bands together with their respective assignments are shown in Table S1. In Fig. 2, the spectrum of the two non-tannin modified hydrogels, **K_borax** and **K_BA,** are compared to that of **KGM** powder, and they show a broad band at 3435 cm^{-1} corresponding to –OH stretching vibrations, indicative of the high hydroxyl group of saccharide content in **KGM**. The characteristic peak at 1734 cm^{-1}, attributed to –C═O stretching vibrations of **KGM**, is significantly reduced in the hydrogel spectra, suggesting successful crosslinking under involvement of the carbonyl functionalities in the hemicellulose matrix, (Kurt & Kahyaoglu, 2017) and/or partial hydrolysis of esters along the **KGM** polymers. The bands between 1620 cm^{-1} and 1608 cm^{-1} are caused by the asymmetric stretching of the $–COO^-$ group (Postulkova et al., 2017). Additionally, the region from 1500 cm^{-1} to 1200 cm^{-1} show coupling of deformation vibrations of groups, such as –C═C, $–CH_2$ and –CHO

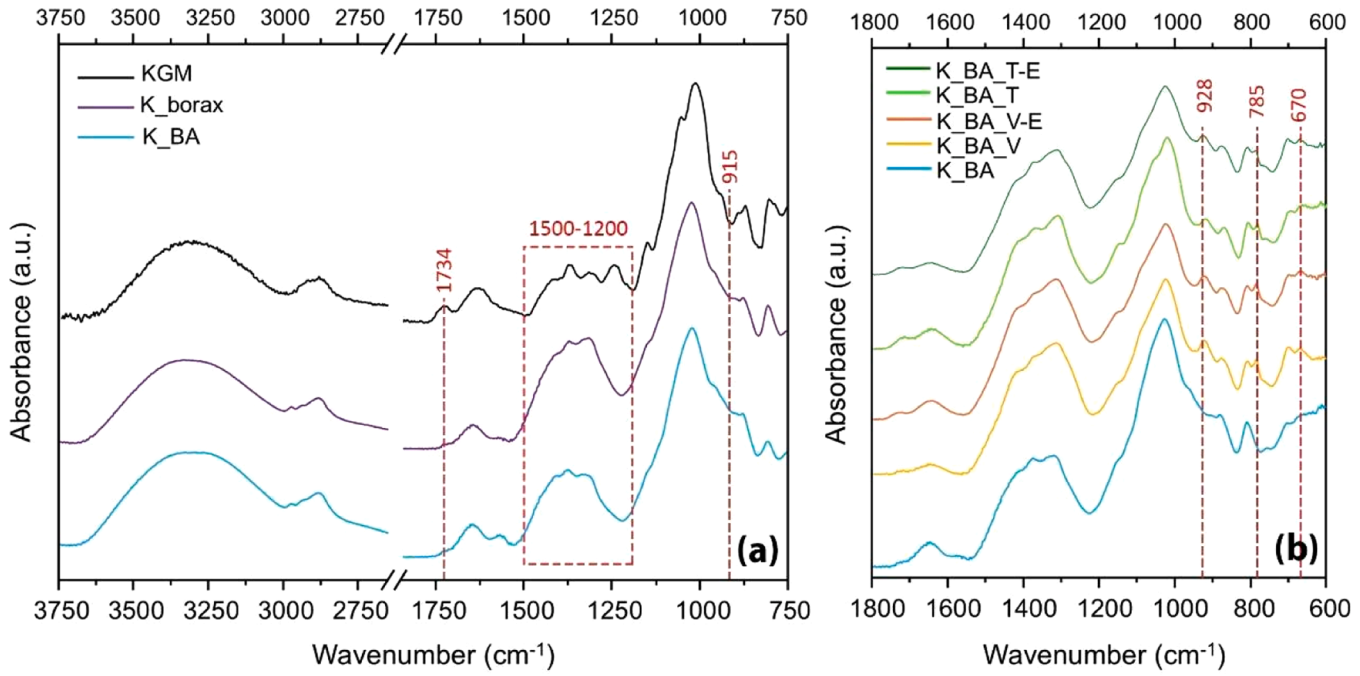

Fig. 2. Spectra obtained with ATR-FTIR of the freeze-dried non-modified hydrogels (a), ***Vv***-modified and **TA** -modified hydrogels, zoomed in the 1800–600 cm^{-1} range (b).

(Anvari et al., 2016; Liu et al., 2021) resulting in more intense bands in the spectra related to **K_borax** and **K_BA**. For the latter hydrogels, the region between 1400 cm^{-1} and 1320 cm^{-1} displays bands associated with the asymmetric stretching of –B–O–C, indicative of diol complexation, while the shoulder around 915 cm^{-1} is attributable to –B–O stretching vibrations (Chaudhary et al., 2020). These absorptions confirm the structural interactions resulting from the crosslinking process in the hydrogels, and thus more importantly also the successful formation of the crosslinking upon *in situ* borax-formation in case of **K_BA**.

In Fig. 2b, the spectrum of the **K_BA** hydrogel is compared with those of tannin-modified hydrogels, *i.e.*, **K_BA_V, K_BA_V-E, K_BA_T** and **K_BA_T-E**. The –OH stretching band shifts to around 3352 cm^{-1} in all tannin-modified hydrogels implying the physical entanglement of tannins within the hydrogel (see Figure S2) (Zhou et al., 2022). The –C═O stretching vibration shifts to 1720 cm^{-1} in **K_BA_V** and **K_BA_V-E**, and to 1715 cm^{-1} in **K_BA_T** and **K_BA_T-E**, indicating tannin presence and incorporation into the polymer matrix (Zhou et al., 2022). Additionally, bands at 1705, 1607, and 1542 cm^{-1}, which correspond to the C═O and C═C stretching vibrations of aromatic esters from the tannins, confirm the presence of the aromatic ester structure within the hydrogels (Zhou et al., 2022). In both ***Vv***- and **TA**-containing hydrogels, bands at 785 and 670 cm^{-1}, are attributed to –C–H out-of-plane bending of the tannin, furtherly confirming its incorporation (Ari et al., 2021). Additionally, the appearance of a defined band at 928 cm^{-1} in both ***Vv***- and

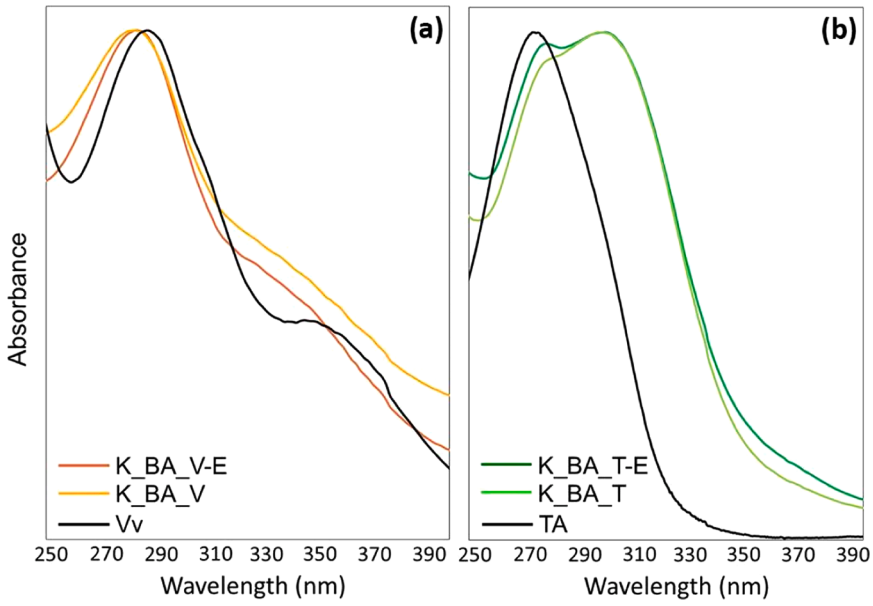

Fig. 3. UV–Vis spectra of aqueous solutions, zoomed in the 250–400 nm range, of ***Vv***-modified hydrogels (a) and **TA**-modified hydrogels (b), compared to their respective plain tannin aqueous solutions.

TA-containing hydrogels, suggests the formation of additional borate-polysaccharide and borate-tannin complexes within the **KGM** tannin-modified hydrogels (Chaudhary et al., 2020).

The tannin-**KGM** interaction was further confirmed by performing UV–Vis spectroscopy on an aqueous solution of tannins ***Vv*** or **TA** at concentrations of 10 ppm and on the hydrogel solutions containing tannins ***Vv*** or **TA** at the same dilution. The spectra in Fig. 3 were normalized to facilitate the observation of the shift in the band related to the $\pi \longrightarrow \pi^*$ transition of polyphenols, which typically lies around 280 nm (Pizzi, 2008). In Figure S3, it is shown that the non-modified hydrogel (**K_BA**) does not exhibit any absorption in that region.

In Fig. 3a, the ***Vv*** spectrum shows a maximum at 284 nm, while the spectra of **K_BA_V** and **K_BA_V-E** display a slight blue-shift, *i.e.*, a shift of the polyphenol-related band to lower wavenumbers. On the contrary, the spectrum of **TA** in water is characterized by a maximum of 275 nm (Fig. 3b), while those of **K_BA_T** and **K_BA_T-E** show red shifts, *i.e.*, a slight shift towards higher wavenumbers. Additionally, a second band appears around 310 nm in the hydrogel spectra, which correspond to the ionized **TA** molecule (Shutava et al., 2005). The shift and the doubling of the bands indicate a change in the symmetry of the polyphenol molecule, providing evidence of the interaction between tannins and the polymeric matrix, only concerning intensity of the bands (Luo et al., 2015). Only little differences are observed between tannin-containing gels with and without **ECH**. This may be due to hydrogen bonding occurring more readily and in considerably higher quantities than the chemical bonding upon epoxide opening (Akagawa & Suyama, 2001).

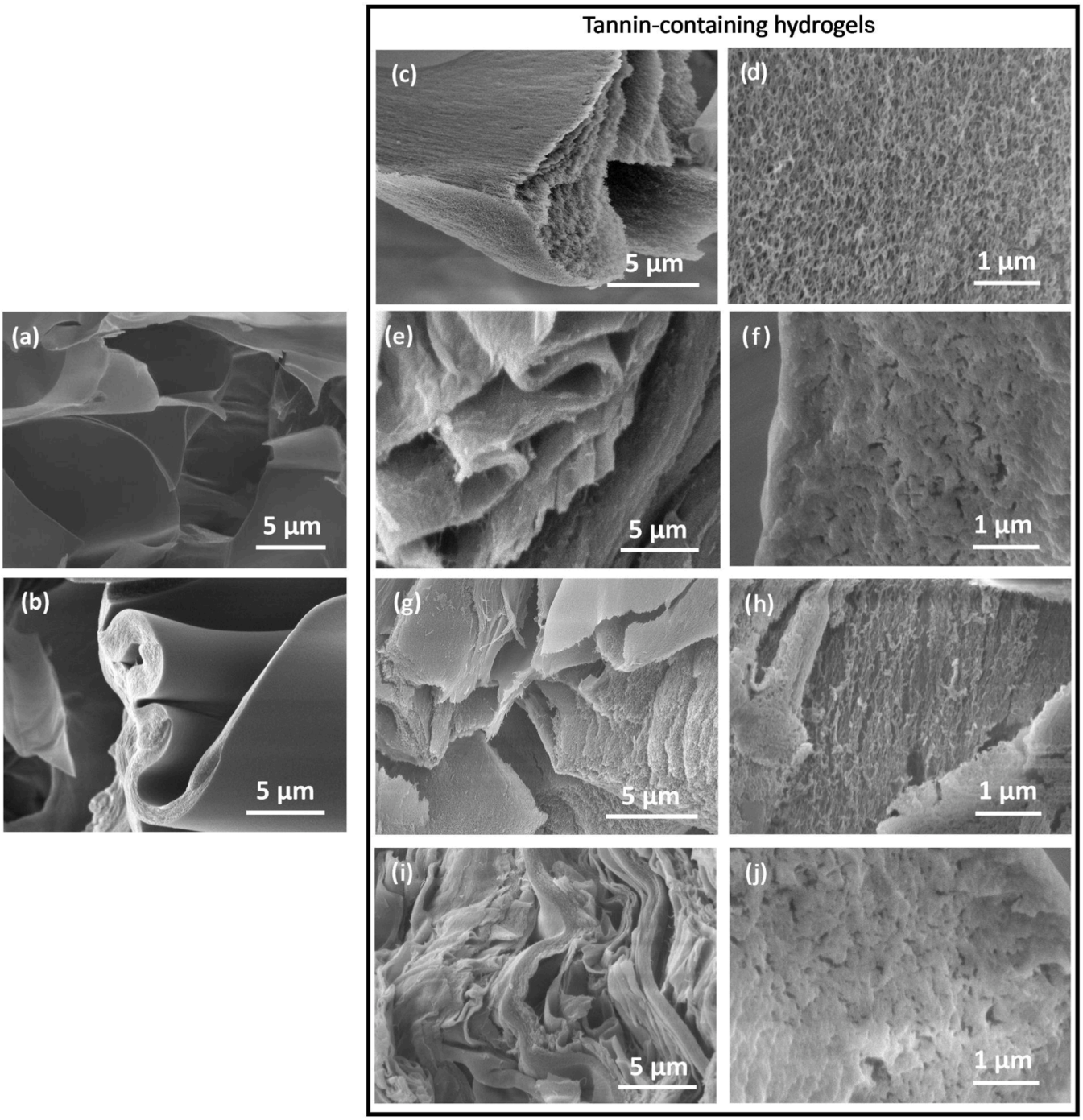

Fig. 4. SEM images of freeze-dried **K_borax** (a), **K_BA** (b), **K_BA_V** (c, d), **K_BA_V-E** (e, f), **K_BA_T** (g, h), **K_BA_T-E** (i, j).

To further examine the effect of the *in situ* borax formation and the consequences of the formulation modifications with tannins and organic crosslinker on the morphology of the gel, all systems were analyzed using SEM. In Figures S4a, b, c, d, e and f, gels display an irregular three-dimensional porous structure typical of **KGM**-borax crosslinking (Li et al., 2015). At higher magnification (Fig. 4a and b), the porous structure of **K_BA** consists of folded sheets with a mean thickness of 1.11 μm (± 0.28), resulting from a denser network than **K_borax**. In fact, the changes in the crosslinking system of **K_BA**, where sodium hydroxide effectively deprotonates both **KGM** and **BA**, enhanced bonding (Mahjoub et al., 2019). The thickening of the sheets occurs in all the *in situ* crosslinked gels (Fig. 4c, e, g, i).

Moreover, the simple addition of tannins, *i.e.*, ***Vv*** or **TA**, respectively, led to the formation of several microporous structures in **K_BA_V** and **K_BA_T** (Fig. 4d and h). These pores, with a mean diameter of 0.12 μm (± 0.02), likely result from hydrogen bonding between the hydroxyl groups of tannins and **KGM** (Feng et al., 2021). In **K_BA_V-E** and **K_BA_T-E,** where the tannins were included with the epoxidating agent, the porous walls densify, forming a thicker, sponge-like structure (Fig. 4f and j) (Ma et al., 2020).

3.2. Optical properties of hydrogels

While having beneficial effects on the microstructure and the stability of the hydrogels as such, the incorporation of tannins in the structure of the gels affected their final coloration and opacity. Given the eventual importance of final coloration and opacity for conservation applications, where a whitish and transparent gel is currently preferred (Micheli et al., 2014; Sansonetti et al., 2020), the colorimetric coordinates and the Contrast Ratio of the tannin-containing gels were measured; data are presented in Table 2. As displayed in Fig. 5a, b and c, the **K_BA** gel appears almost transparent, while the addition of ***Vv*** tannin results in a deep red coloration as attested by the high and positive of redness/greenness a* values, +25.93 for **K_BA_V** and +26.7 for **K_BA_V-E**, while **TA** addition causes them to become greenish, as defined by negative value of a* -3.61 for **K_BA_T**-2.75 for **K_BA_T-E**, due to color variation that **TA** undergoes as a function of environmental pH and the intermolecular interactions of **TA** in the matrix. No variation in the yellow–blue, b*yellowness/blueness, was detected between ***Vv*****-** and **TA**-based systems, while coloration of the first ones results lighter, L*: lightness/darkness parameter, than these last. However, to get reliable information on the opacity, the Contrast Ratio was assessed showing significant different values among ***Vv***- and **TA**-containing hydrogels. **TA**-containing hydrogels (**K_BA_T** and **K_BA_T-E**) display a lower Contrast Ratio than those containing ***Vv*** (**T_BA_V** and **K_BA_V-E**) implying a major transparency for **TA** samples.

It is also interesting to notice how the gels additionally crosslinked with **ECH**, *i.e.*, **K_BA_V-E** and **K_BA_T-E**, exhibit higher contrast ratio and thus higher opacity, indicating that the denser pores observed in the SEM analysis affect the opacity.

3.3. Radical scavenging activity of hydrogels

The radical scavenging activity, correlated to the antioxidant activity of the tannin-modified hydrogels **K_BA_V, K_BA_V-E, K_BA_T**, and **K_BA_T-E** were measured using the **DPPH** radical scavenging assay. For the measurements were used freeze-dried samples of the various hydrogels. For the hydrogels **K_BA_V, K_BA_V-E, K_BA_T**, and **K_BA_T-E,** moderate activities were found, in form of IC_{50} values of 107 mg/L, 112 mg/L, 110 mg/L, and 111 mg/L, respectively. A control sample of gallic acid, run as control during the analyses, was found to exhibit an IC_{50} of 35 mg/L. The measured values suggest that crosslinking is not fully consuming phenolic hydroxyl groups, allowing for a useful antioxidant activity of the realized hydrogels.

Table 2
Chromatic coordinates (CIELAB) of the tannin-modified hydrogels and their Contrast Ratio. a*: redness/greenness, b*: yellowness/blueness, L*: lightness/darkness.

Hydrogel	a*	b*	L*	Contrast Ratio (%)
K_BA_V	25.9 (± 0.2)	39.5 (± 0.3)	48.8 (± 0.1)	17.7 (± 0.5)
K_BA_V-E	26.7 (± 0.3)	37.6 (± 0.3)	45.5 (± 0.4)	19.0 (± 0.4)
K_BA_T	-3.6 (± 0.1)	38.9 (± 0.0)	74.4 (± 0.2)	7.8 (± 0.2)
K_BA_T-E	-2.8 (± 0.1)	36.0 (± 0.3)	72.5 (± 0.2)	9.5 (± 0.1)

3.4. Moisture properties of hydrogels

The moisture properties of these gels are summarized in the table in Fig. 6b. Interestingly, the bivariate plot of SC and RC in Fig. 6 reveals distinct trends within the tannin-modified gels, both with or without additional **ECH** crosslinking. In fact, both RC, which indicates the ability of the network to retain water (the higher the value, the lower the retention), and SC, which provides the percentage of solvent absorbed by the gel network, highlighted a remarkable difference between **K_BA** and **K_borax**, and between tannin-modified gels with/without **ECH**. The plot clearly showed that **K_borax** is the system with the highest SC and RC ($2.2 \pm 0.5 \times 10^2$ % and 43.2 ± 1.0 mg cm^{-2}, respectively) indicating a highly expansive network as well as significant water release. Meanwhile, **K_BA** displays significantly lower values of SC ($1.2 \pm 0.2 \times 10^2$ %) and RC (18.1 ± 1.0 mg cm^{-2}) suggesting a more constrained structure, due to the thicker and denser structure provided by the *in situ* gelation process (see Section 3.1, Fig. 4a and b). This structure exhibit an improved ability to retain water in comparison with **K_borax**, hinting at the beneficial effect of a tighter crosslinking and eventually even more hydrophilic surfaces due to an increased amount of deprotonated hydroxyl groups throughout the matrix.

Moreover, the plot effectively shows how the cross-linking process between tannins and the polymer influences the moisture properties of the final gel formulation. In this regard, a clear distinction was observed for the modified gels cross-linked with or without **ECH. K_BA_V** and **K_BA_T**, both containing tannins bonded with KGM physically via hydrogen bonding and chemically via the formation of the borax-type bridge, presented SC and RC values similar to each other, clustering together. These values are substantially higher than **K_BA**, suggesting that the incorporation of tannins enhances hydrophilicity, but slightly decreases their water-retention ability, probably due to the influence in the microporosity and the increment of hydrophilic functionalization (Kim et al., 2020; Mahjoub et al., 2019). Conversely, **K_BA_V-E** and **K_BA_T-E** exhibited SC values similar, grouping together, to their non-epoxidized counterparts ($2.0 \pm 0.6 \times 10^3$ % and $2.0 \pm 0.1 \times 10^3$ %, respectively), but the reduction in RC proved enhancement in the water-release ability. This behavior can be attributed to the structural effects of **ECH**. The covalent bonding introduced by the organic crosslinker likely results in a denser and more compact network that increases matrix thickness and reduces free volume, thereby creating more tortuous diffusion paths for solvent molecules. Additionally, this denser architecture may slightly reduce surface wettability, collectively contributing to more controlled water release despite high water uptake (Dabbaghi et al., 2019).

The results obtained from the biplot are confirmed by the water release/water uptake ratio (WR/WU) revealing that **K_BA_T-E** and **K_BA_V-E** emerge as the best candidates for cleaning applications in the field of cultural heritage, since they offer the advisable combination of high swelling capacity and low retention capability.

EWC is consistently high (92–95 %) across all formulations, reflecting their overall strong hydrophilic nature, and follows the same trend as SC, supporting comparable interpretations.

3.5. Thermal properties of hydrogels

The differences in the formulations of the hydrogels, and here

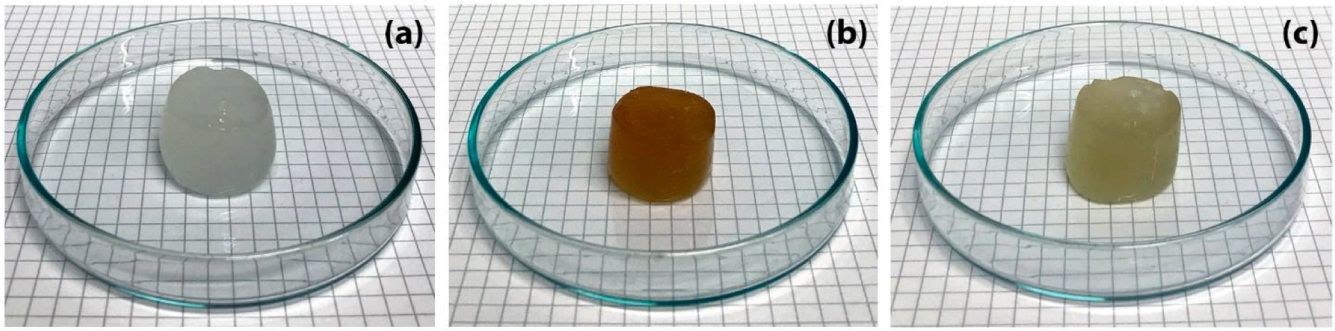

Fig. 5. **KGM** hydrogel with the optimized crosslinking system **K_BA** (a), and with tannin modification **K_BA_V** (b) and **K_BA_T** (c).

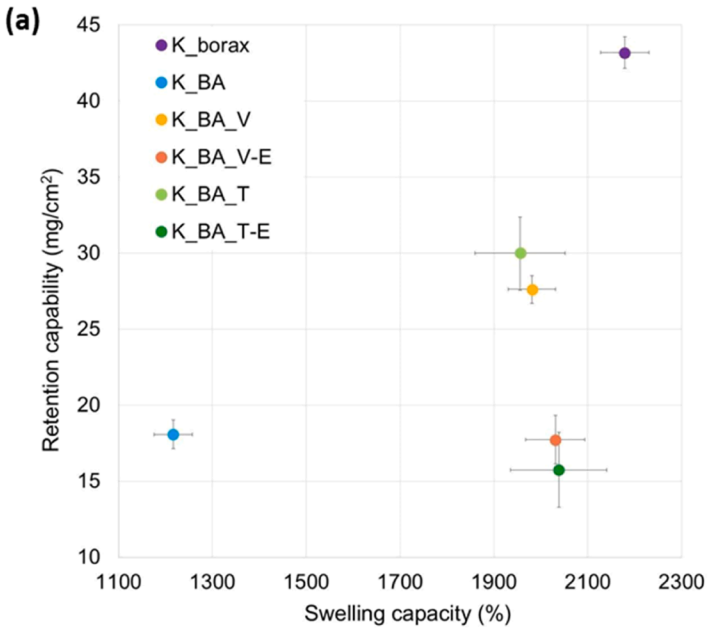

(b)

Hydrogel	EWC (%)	WR/WU (%)	SC (× 10³) (%)	RC (mg cm⁻²)
K_borax	95.59 (± 0.21)	13.5 (± 0.6)	2.18 (± 0.05)	43 (± 1)
K_BA	92.40 (± 0.07)	12.2 (± 0.4)	1.22 (± 0.02)	18 (± 1)
K_BA_V	95.17 (± 0.23)	14.1 (± 0.6)	1.98 (± 0.05)	27.6 (± 0.9)
K_BA_V-E	95.3 (± 0.3)	9.2 (± 0.7)	2.03 (± 0.06)	17.7 (± 1.6)
K_BA_T	95.44 (± 0.19)	15.22 (± 0.20)	1.96 (± 0.10)	30.0 (± 2.4)
K_BA_T-E	95.2 (± 0.5)	10.33 (± 0.16)	2.04 (± 0.10)	15.7 (± 2.5)

Fig. 6. Bivariate plot of swelling capacity (SC) and retention capability (RC) values (a), and overview of moisture properties of the gels: swelling capacity (SC), retention capability (RC), equilibrium water content (EWC) and water release/water uptake ratio (WR/WU) (The average values and the related standard deviations were determined by repeating the experiment five times) (b).

especially in the presence of crosslinking elements and in the structure-variating tannins, were expected to have only a subtle impact on thermal properties of the various hydrogels, and thus on their stability under various temperatures. Thermal analyses in the form of TGA and DSC were hence performed, and developments of mass losses and heat flow curves are displayed in Fig. 7. The maximum temperature of the degradation steps (T_{max}) from TGA and residue and glass transition temperature (T_g) from DSC are given in the table in Fig. 7d

Data confirm that the *in situ* formation of the borax-based crosslinking system gives a more homogeneous and thus slightly more stable hydrogel that seems to retain more effectively structural waters still left in the structures after the freeze-drying, causing a higher temperature for the initial moisture-loss in the TGA for **K_BA**, 90 °C, in comparison to **K_borax**, 77 °C. Adding the tannins ***Vv*** and **TA** to the basic formulation mixture causes a reduction in the onset temperature, $\Delta T = 16$ °C, of the moisture loss, and a general reduction of thermal stability. A slither decrease is observed for the addition of **ECH**. All samples exhibit similar ash contents, indicating the overall consistency of the preparations in terms of inorganic, *i.e.*, boron content.

DSC analyses display for all samples a T_g at around 187–188 °C (Fig. 7c), indicative for the crosslinking involving the hydroxyl groups of the carbohydrates (Enomoto-Rogers et al., 2013). Noteworthy is the

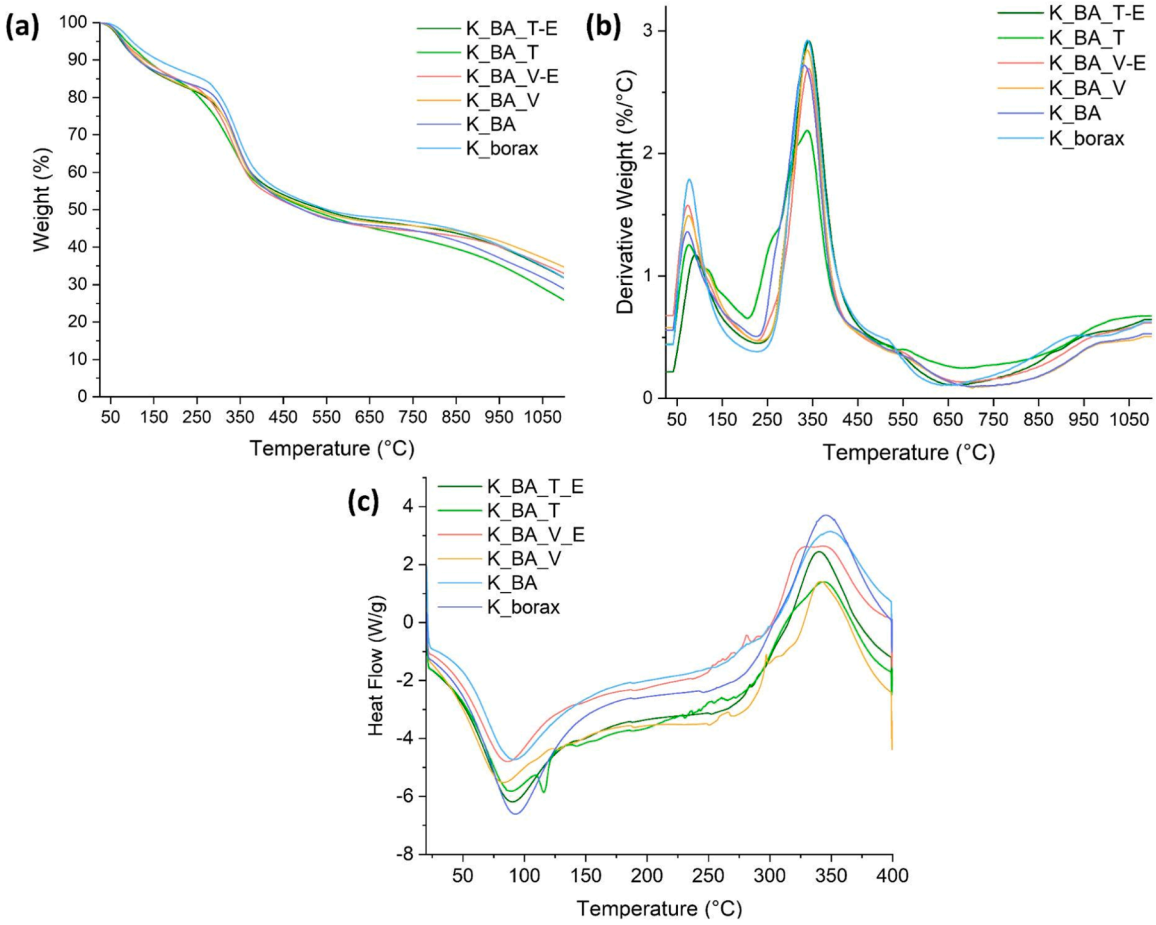

(d)

	TGA				DSC
	T_{max_1} (°C)	T_{max_2} (°C)	T_{max_3} (°C)	Residue (%)	T_g (°C)
K_borax	77	---	340	32	188
K_BA	90	---	340	29	188
K_BA_V	74	---	338	35	187
K_BA_V-E	71	263 (sh)	331	33	187
K_BA_T	74	225 (sh)	339	25	187
K_BA_T-E	74	---	340	32	188

Fig. 7. Thermogravimetric (TG) curves (a) and their corresponding derivatives (DTGA) (b); first heating heat flows measured by DSC (c); maximum temperature of the degradation step (T_{max}) from TGA and residue and glass transition temperature (T_g) from DSC of the realised hydrogels (d).

clearly visible endothermic peak for the sample **K_BA_T** at 116 °C, possibly indicating for this sample a reduced compatibility between the polymer and the additive **TA**. Such indication of a potential structural incompatibility is observed also for **K_BA_V**, albeit much less pronounced, causing only a shoulder in the curve at around 128 °C. Interestingly, when adding **ECH** to the samples, the incompatibility seems to be mediated, resulting in the loss of these endothermic peaks for **K_BA_T-E** and **K_BA_V-E**. The visible changes in the gelation enthalpies across the various hydrogels reflect nicely the differences caused in terms of structural ordering upon addition of the two different tannins, causing a disruption of the crystallinity of the **KGM** samples strong enough to be monitored. Interestingly, DSC curves for the tannin containing hydrogels show also exothermic peaks at temperatures around 340 °C, with onsets at around 280 °C, indicative of a polymerization before finally thermal degradation in form of random condensation starts as already indicated by the TGA data (Fig. 7d). Samples **K_BA_V-E** and **K_BA_T** show clear maxima, while samples **K_BA_V** and **K_BA-T-E** exhibit only shoulders in their heat flow curves. The high temperature found for this exothermic peak suggests that this polymerization can be imagined as 'random' or cascade-type polycondensation reactions involving both the polyphenols and the polysaccharides in inter- and intramolecular fashion. The roughness of the curves for tannin-containing samples in the temperature interval between 225 °C and 280 °C can be explained with intensifying interactions between the polymers and the onset of condensations involving the hydroxyl groups of both the tannins ***Vv*** and **TA** and **KGM**, leading to a more pronounced polymerization in form of single condensations across species causing a first distinctive exothermic peak, for example for samples **K_BA_V-E** and **K_BA_T-E** at *circa* 295 °C.

3.6. *Mechanical properties of hydrogels*

The mechanical performance of the newly synthesized gels was evaluated through tensile strength, elongation at break and hardness, as

described in Section 2.12.

As displayed in Fig. 8a, c and d, the incorporation of tannins in **K_BA_V** and **K_BA_T** significantly improved tensile strength, compressive resistance and Young modulus compared to **K_BA**. These enhancements reflect a better balance between flexibility and structural integrity. The compressive stress–strain curves (Figure S5b) confirm this trend: **K_BA** exhibited a shallow slope, indicative of low toughness, while tannin-containing gels demonstrated steeper slopes under higher strain levels. This improvement was particularly notable in gels containing **TA**, which possesses a higher hydroxyl content than ***Vv***, providing more binding sites for stronger intermolecular interactions within the gel matrix (Chen et al., 2016; Gwak et al., 2021). Additionally, the introduction of **ECH** further reinforces the gels network, by forming stable covalent bonds, leading to increased hardness and mechanical strength (Nicu et al., 2024). This is supported by tensile stress–strain data (Figure S5a), which show that the **K_BA_T-E** undergoes significant deformation up to the yield point, presenting high ductility with minimal brittleness. In contrast, the base **K_BA** exhibits gradual yield and moderate decline, indicating reduced elasticity and lower fracture resistance. Compressive stress-strain curves (Figure S5b) reveal that **K_BA_T-E** has steeper slopes at higher strain levels and shows strain-hardening behavior, increasing its resistance to deformation. The enhanced mechanical performance can be attributed to the synergistic interaction between the hydroxyl-rich structure presented by **TA** and **ECH** crosslinking, resulting in a dense, resilient network. While it shows a relatively high standard deviation in hardness, making interpretation less straightforward, its mechanical behavior is still notable (Fig. 8b). The increased crosslinking, however, also limited chain mobility, leading to reduced elongation at break.

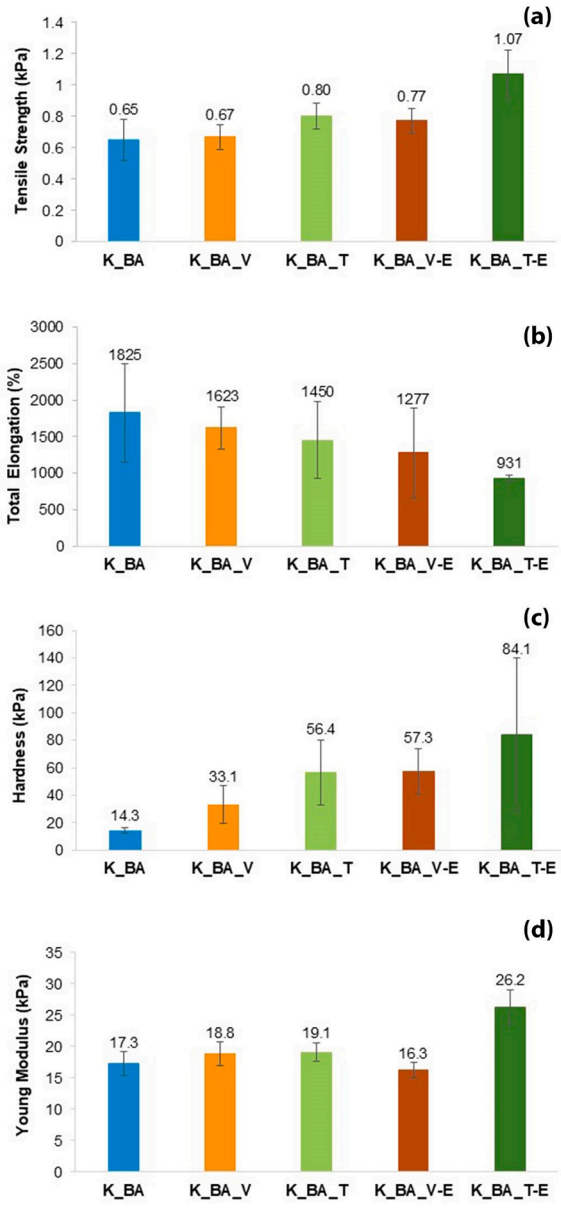

Fig. 8. Tensile strength (a), elongation (b) (mean values ± SE; $n = 3$), hardness (c) and Young modulus (d) values calculated for different soft gels (mean values ± SE; $n = 3$).

When comparing these findings to previous studies on hydrogels commonly used for artwork cleaning, *i.e.*, Agar gel, a significant improvement is evident. Agar gel is known for its brittleness in cleaning application, with a reported elongation at break of only 11.8 ± 0.1 % (Lee et al., 2023), which is substantially lower than the values observed for our newly formulated gels, as shown in Fig. 8b. This comparison underscores the advantages of gels containing tannins and **ECH** (**K_BA_V_E** and **K_BA_T_E**), particularly for applications that demand enhanced durability and strength, while still achieving a balance of flexibility in the material.

4. Conclusions

In this study, KGM-based hydrogels crosslinked on the basis of newly developed *in situ* borax approach were developed, exhibiting a much more homogeneous matrix than hydrogels realized using directly borax. Additionally, the incorporation of tannins into the crosslinked matrix, using the *in situ* borax crosslinking approach changed in crosslinking degree and nature, adding a more lipophilic compound in comparison to the sole boron crosslinker. *In situ* borax as a crosslinking system during gel preparation altered the microstructure by thickening the structural sheets. Consequently, the moisture, mechanical and thermal properties were affected, resulting in reduced hydrophilicity, greater control over solvent release, and increased extensibility in **K_BA** gel compared to **K_borax**.

The addition of tannins, both condensed or hydrolysable, enhanced the moisture and mechanical properties of the gels. Addition of tannins led to the resulting **K_BA_V** and **K_BA_T** gels exhibiting increased hydrophilicity and diminished solvent release compared to **K_BA**. Mechanically, these gels displayed higher tensile strength and hardness, along with reduced extensibility. Thermally, the various hydrogels exhibit subtle differences that are in line with the structural variations.

Employing additionally **ECH** for achieving an additional crosslinking with modification of hydrophobicity led to gels **K_BA_V-E** and **K_BA_T-E** that exhibited lower hydrophilicity and greater control over solvent release, while also displaying enhanced tensile strength and hardness. Realized tannin-containing hydrogels exhibit radical scavenging activities.

With **K_BA_T-E** featuring important properties like chemical inertness, ability to absorb a significant amount of solvent, effectively regulating solvent release, and being resistant to breakage based on sufficient structural flexibility, current efforts aim to evaluate this gel together with suitable controls in cleaning applications in the cultural heritage sector.

CRediT authorship contribution statement

Eleonora Verni: Writing – original draft, Visualization, Methodology, Investigation. **Francesca Sabatini:** Methodology, Formal analysis, Data curation. **Chaehoon Lee:** Writing – review & editing, Validation, Methodology. **Giacomo Fiocco:** Visualization, Validation, Supervision. **Maduka Lankani Weththimuni:** Writing – review & editing, Validation. **Barbara Vigani:** Formal analysis, Data curation. **Heiko Lange:** Writing – review & editing, Supervision, Resources, Methodology, Data

curation, Conceptualization. **Marco Malagodi:** Writing – review & editing, Validation, Supervision, Resources, Project administration. **Francesca Volpi:** Writing – review & editing, Validation, Methodology.

Declaration of competing interest

The authors declare that they have no known competing financial interests or personal relationships that could have appeared to influence the work reported in this paper.

The author is an Editorial Board Member/Editor-in-Chief/Associate Editor/Guest Editor for this journal and was not involved in the editorial review or the decision to publish this article.

Acknowledgements

The project is funded under the National Recovery and Resilience Plan (NRRP), Mission 4 Component 2 Investment 1.4 - Call for tender No. 3138 of 16 December 2021, rectified by Decree n.3175 of 18 December 2021 of Italian Ministry of University and Research funded by the European Union – Next Generation EU; Award Number: Project code CN_00000033, Concession Decree No. 1034 of 17 June 2022 adopted by the Italian Ministry of University and Research, CUP H43C22000530001, Project title "National Biodiversity Future Center - NBFC". The Program PON Ricerca e Innovazione 2014-2020 FSE REACT-EU Azione IV.6 of the Italian Ministry of University and Research, CUP F11B21009210007, is also acknowledged.

Supplementary materials

Supplementary material associated with this article can be found, in the online version, at doi:10.1016/j.carpta.2025.100875.

Data availability

Data will be made available on request.

References

Akagawa, M., & Suyama, K. (2001). Amine oxidase-like activity of polyphenols. *European Journal of Biochemistry, 268*, 1953–1963. https://doi.org/10.1046/j.1432-1327.2001.02068.x

Alavarse, A. C., Frachini, E. C. G., da Silva, R. L. C. G., Lima, V. H., Shavandi, A., & Petri, D. F. S. (2022). Crosslinkers for polysaccharides and proteins: Synthesis conditions, mechanisms, and crosslinking efficiency, a review. *International Journal of Biological Macromolecules, 202*, 558–596. https://doi.org/10.1016/j.ijbiomac.2022.01.029

Alfonsi, E., Lange, H., Zongo, L., Poce, G., Sgarzi, M., & Crestini, C. (2023). Tannin microcapsules for synergy-enhanced sunscreen formulations. *Industrial Crops and Products, 192*, Article 116105. https://doi.org/10.1016/j.indcrop.2022.116105

Anvari, M., Tabarsa, M., Cao, R., You, S., Joyner (Melito), H. S., Behnam, S., & Rezaei, M. (2016). Compositional characterization and rheological properties of an anionic gum from *Alyssum homolocarpum* seeds. *Food Hydrocolloids, 52*, 766–773. https://doi.org/10.1016/j.foodhyd.2015.07.030

Ari, B., Sahiner, M., Demirci, S., & Sahiner, N. (2021). Poly(vinyl alcohol)-tannic acid cryogel matrix as antioxidant and antibacterial material. *Polymers, 14*, 70. https://doi.org/10.3390/polym14010070

Bell, B. M., Briggs, J. R., Campbell, R. M., Chambers, S. M., Gaarenstroom, P. D., Hippler, J. G., Hook, B. D., Kearns, K., Kenney, J. M., Kruper, W. J., Schreck, D. J., Theriault, C. N., & Wolfe, C. P. (2008). Glycerin as a renewable feedstock for epichlorohydrin production. The GTE process. *CLEAN – Soil, Air, Water, 36*, 657–661. https://doi.org/10.1002/clen.200800067

Borysenko, M., 2021. Gels: effective instruments for cleaning of graphical works 4.

Buzzini, P., Arapitsas, P., Goretti, M., Branda, E., Turchetti, B., Pinelli, P., Ieri, F., & Romani, A. (2008). Antimicrobial and antiviral activity of hydrolysable tannins. *MRMC, 8*, 1179–1187. https://doi.org/10.2174/138955708786140990

Chaudhary, J. P., Kholiya, F., Vadodariya, N., Budheliya, V. M., Gogda, A., & Meena, R. (2020). Carboxymethylagarose-based multifunctional hydrogel with super stretchable, self-healable having film and fiber forming properties. *Arabian Journal of Chemistry, 13*, 1661–1668. https://doi.org/10.1016/j.arabjc.2017.12.034

Chelazzi, D., Bordes, R., Giorgi, R., Holmberg, K., & Baglioni, P. (2020). The use of surfactants in the cleaning of works of art. *Current Opinion in Colloid & Interface Science, Surfactants, 45*, 108–123. https://doi.org/10.1016/j.cocis.2019.12.007

Chen, Y., Song, C., Lv, Y., & Qian, X. (2019). Konjac glucomannan/kappa carrageenan interpenetrating network hydrogels with enhanced mechanical strength and excellent self-healing capability. *Polymer, 184*, Article 121913. https://doi.org/10.1016/j.polymer.2019.121913

Chen, Y.-N., Peng, L., Liu, T., Wang, Y., Shi, S., & Wang, H. (2016). Poly(vinyl alcohol)–Tannic acid hydrogels with excellent mechanical properties and shape memory behaviors. *ACS Appl. Mater. Interfaces, 8*, 27199–27206. https://doi.org/10.1021/acsami.6b08374

Chmara, M.H., 2024. Synthesis, rheology, and biocompatibility of dynamic covalent borax hydrogels.

Dabbaghi, A., Kabiri, K., Ramazani, A., Zohuriaan-Mehr, M. J., & Jahandideh, A. (2019). Synthesis of bio-based internal and external cross-linkers based on tannic acid for preparation of antibacterial superabsorbents. *Polymers for Advanced Technologies, 30*, 2894–2905. https://doi.org/10.1002/pat.4722

Davé, V., & McCarthy, S. P. (1997). Review of konjac glucomannan. *Journal of Environmental Polymer Degradation, 5*, 237–241. https://doi.org/10.1007/BF02763667

Domingues, J., Bonelli, N., Giorgi, R., & Baglioni, P. (2014). Chemical semi-IPN hydrogels for the removal of adhesives from canvas paintings. *Appl. Phys. A, 114*, 705–710. https://doi.org/10.1007/s00339-013-8150-0

Enomoto-Rogers, Y., Ohmomo, Y., & Iwata, T. (2013). Syntheses and characterization of konjac glucomannan acetate and their thermal and mechanical properties. *Carbohydrate Polymers, 92*, 1827–1834. https://doi.org/10.1016/j.carbpol.2012.11.043

Ervina, A., Santoso, J., Prasetyo, B. F., Setyaningsih, I., & Tarman, K. (2020). Formulation and characterization of body scrub using marine alga Halimeda macroloba, chitosan and konjac flour. *IOP Conference Series: Earth and Environmental Science, 414*, Article 012004. https://doi.org/10.1088/1755-1315/414/1/012004

Feng, X., Hou, X., Cui, C., Sun, S., Sadik, S., Wu, S., & Zhou, F. (2021). Mechanical and antibacterial properties of tannic acid-encapsulated carboxymethyl chitosan/polyvinyl alcohol hydrogels. *Engineered Regeneration, 2*, 57–62. https://doi.org/10.1016/j.engreg.2021.05.002

Ferruti, F., Pylypchuk, I., Zoia, L., Lange, H., Orlandi, M., Moreno, A., & H Sipponen, M. (2023). Recombinatorial approach for the formation of surface-functionalised alkaline-stable lignin nanoparticles and adhesives. *Green Chemistry, 25*, 639–649. https://doi.org/10.1039/D2GC03406A

Fiocco, G., Invernizzi, C., Rovetta, T., Albano, M., Malagodi, M., Davit, P., & Gulmini, M. (2021). Surfing through the coating system of historic bowed instruments: A spectroscopic perspective. *Spectroscopy Europe, 19*. https://doi.org/10.1255/sew.2021.a8

Fraga-Corral, M., Otero, P., Cassani, L., Echave, J., Garcia-Oliveira, P., Carpena, M., Chamorro, F., Lourenço-Lopes, C., Prieto, M. A., & Simal-Gandara, J. (2021). Traditional applications of tannin rich extracts supported by scientific data: Chemical composition, bioavailability and bioaccessibility. *Foods, 10*, 251. https://doi.org/10.3390/foods10020251

Gao, S., Guo, J., & Nishinari, K. (2008). Thermoreversible konjac glucomannan gel crosslinked by borax. *Carbohydrate Polymers, 72*, 315–325. https://doi.org/10.1016/j.carbpol.2007.08.015

Giannì, P., Lange, H., Bianchetti, G., Joos, C., Brogden, D. W., & Crestini, C. (2020). Deposition efficacy of natural and synthetic antioxidants on fabrics. *Applied Sciences, 10*, 6213. https://doi.org/10.3390/app10186213

Gómez, B., Míguez, B., Yáñez, R., & Alonso, J. L. (2017). Manufacture and properties of glucomannans and glucomannooligosaccharides derived from konjac and other sources. *Journal of Agricultural and Food Chemistry, 65*, 2019–2031. https://doi.org/10.1021/acs.jafc.6b05409

Gwak, M. A., Hong, B. M., Seok, J. M., Park, S. A., & Park, W. H. (2021). Effect of tannic acid on the mechanical and adhesive properties of catechol-modified hyaluronic acid hydrogels. *International Journal of Biological Macromolecules, 191*, 699–705. https://doi.org/10.1016/j.ijbiomac.2021.09.123

Halim, Y., Angelina, B., Hardoko, H., & Handayani, R. (2023). Characteristics of dried noodle analogue made from sorghum flour and rice flour added with konjac glucomannan. *IOP Conference Series: Earth and Environmental Science, 1200*, Article 012032. https://doi.org/10.1088/1755-1315/1200/1/012032

Haslam, E. (1989). Plant polyphenols: Vegetable tannins revisited. *CUP Archive*.

Hurler, J., Engesland, A., Poorahmary Kermany, B., & Škalko-Basnet, N. (2012). Improved texture analysis for hydrogel characterization: Gel cohesiveness, adhesiveness, and hardness. *Journal of Applied Polymer Science, 125*, 180–188. https://doi.org/10.1002/app.35414

Inokoshi, S., Burrow, M. F., Kataumi, M., Yamada, T., & Takatsu, T. (1996). Opacity and color changes of tooth-colored restorative materials. *Operative Dentistry, 21*, 73–80.

Jafari, H., Ghaffari-Bohlouli, P., Vahid Niknezhad, S., Abedi, A., Izadifar, Z., Mohammadinejad, R., Varma, S. R., & Shavandi, A. (2022). Tannic acid: A versatile polyphenol for design of biomedical hydrogels. *Journal of Materials Chemistry B, 10*, 5873–5912. https://doi.org/10.1039/D2TB01056A

John, B., & Colin, D. H. (2013). Chapter six - catalysis or convenience? Perborate in context. In R. van Eldik, & C. D. Hubbard (Eds.), *Advances in inorganic chemistry, homogeneous catalysis* (pp. 217–310). Academic Press. https://doi.org/10.1016/B978-0-12-404582-8.00006-7.

Khanbabaee, K., & van Ree, T. (2001). Tannins: Classification and definition. *Natural Product Reports, 18*, 641–649. https://doi.org/10.1039/B101061L

Kim, S.-H., Kim, K., Kim, B. S., An, Y.-H., Lee, U.-J., Lee, S.-H., Kim, S. L., Kim, B.-G., & Hwang, N. S. (2020). Fabrication of polyphenol-incorporated anti-inflammatory hydrogel via high-affinity enzymatic crosslinking for wet tissue adhesion. *Biomaterials, 242*, Article 119905. https://doi.org/10.1016/j.biomaterials.2020.119905

Koleckar, V., Kubikova, K., Rehakova, Z., Kuca, K., Jun, D., Jahodar, L., & Opletal, L. (2008). Condensed and hydrolysable tannins as antioxidants influencing the health.

Mini-Reviews in Medicinal Chemistry, 8, 436–447. https://doi.org/10.2174/138955708784223486

Kuniak, L., & Marchessault, R. H. (1972). Study of the crosslinking reaction between epichlorohydrin and starch. *Starch - Stärke, 24*, 110–116. https://doi.org/10.1002/star.19720240404

Kurt, A., & Kahyaoglu, T. (2017). Purification of glucomannan from salep: Part 2. Structural characterization. *Carbohydrate Polymers, 169*, 406–416. https://doi.org/10.1016/j.carbpol.2017.04.052

Lee, C., Di Turo, F., Vigani, B., Weththimuni, M. L., Rossi, S., Beltram, F., Pingue, P., Licchelli, M., Malagodi, M., Fiocco, G., & Volpi, F. (2023). Biopolymer gels as a cleaning system for differently featured wooden surfaces. *Polymers, 15*, 36. https://doi.org/10.3390/polym15010036

Lee, C., Fiocco, G., Vigani, B., Recca, T., Milanese, C., Delledonne, C., Licchelli, M., Rossi, S., Chung, Y., Volpi, F., Weththimuni, M. L., & Malagodi, M. (2024a). Chemically crosslinked alginate hydrogel with polyaziridine: Effects on physicochemical properties and promising applications. *ChemPlusChem.* , Article e202400649. https://doi.org/10.1002/cplu.202400649

Lee, C., Fiocco, G., Vigani, B., Recca, T., Rossi, S., Licchelli, M., Malagodi, M., Weththimuni, M. L., & Volpi, F. (2024b). Retentive bio-based chemical gel for removing glues from water-sensitive wooden artworks. *Journal of Cultural Heritage, 68*, 9–16. https://doi.org/10.1016/j.culher.2024.05.005

Lee, C., Volpi, F., Fiocco, G., Weththimuni, M. L., Licchelli, M., & Malagodi, M. (2022). Preliminary cleaning approach with Alginate and Konjac Glucomannan polysaccharide gel for the surfaces of East Asian and Western string musical instruments. *Materials, 15*, 1100. https://doi.org/10.3390/ma15031100

Li, Z., Su, Y., Xie, B., Liu, X., Gao, X., & Wang, D. (2015). A novel biocompatible double network hydrogel consisting of konjac glucomannan with high mechanical strength and ability to be freely shaped. *Journal of Materials Chemistry. B, 3*, 1769–1778. https://doi.org/10.1039/C4TB01653J

Liao, J., Brosse, N., Pizzi, A., & Hoppe, S. (2019). Dynamically cross-linked tannin as a reinforcement of polypropylene and UV protection properties. *Polymers, 11*, 102. https://doi.org/10.3390/polym11010102

Liu, C., Lei, F., Li, P., Wang, K., & Jiang, J. (2021a). A review on preparations, properties, and applications of cis-ortho-hydroxyl polysaccharides hydrogels crosslinked with borax. *International Journal of Biological Macromolecules, 182*, 1179–1191. https://doi.org/10.1016/j.ijbiomac.2021.04.090

Liu, Z., Ren, X., Cheng, Y., Zhao, G., & Zhou, Y. (2021b). Gelation mechanism of alkali induced heat-set konjac glucomannan gel. *Trends in Food Science & Technology, 116*, 244–254. https://doi.org/10.1016/j.tifs.2021.07.025

Luan, J., Wu, K., Li, C., Liu, J., Ni, X., Xiao, M., Xu, Y., Kuang, Y., & Jiang, F. (2017). pH-sensitive drug delivery system based on hydrophobic modified konjac glucomannan. *Carbohydrate Polymers, 171*, 9–17. https://doi.org/10.1016/j.carbpol.2017.04.094

Luo, J., Zhang, N., Lai, J., Liu, R., & Liu, X. (2015). Tannic acid functionalized graphene hydrogel for entrapping gold nanoparticles with high catalytic performance toward dye reduction. *Journal of Hazardous Materials, 300*, 615–623. https://doi.org/10.1016/j.jhazmat.2015.07.079

Ma, M., Zhong, Y., & Jiang, X. (2020). Thermosensitive and pH-responsive tannin-containing hydroxypropyl chitin hydrogel with long-lasting antibacterial activity for wound healing. *Carbohydrate Polymers, 236*, Article 116096. https://doi.org/10.1016/j.carbpol.2020.116096

Mahjoub, H. F., Zammali, M., Abbes, C., & Othman, T. (2019). Microrheological study of PVA/borax physical gels: Effect of chain length and elastic reinforcement by sodium hydroxide addition. *Journal of Molecular Liquids, 291*, Article 111272. https://doi.org/10.1016/j.molliq.2019.111272

Micheli, L., Mazzuca, C., Cervelli, E., & Palleschi, A. (2014). New strategy for the cleaning of paper artworks: A smart combination of gels and biosensors. *Advances in Chemistry, 2014*, Article 385674. https://doi.org/10.1155/2014/385674

Ming Kuo, S., Jen Chang, S., & Jiin Wang, Y. (1999). Properties of PVA-AA cross-linked HEMA-based hydrogels. *Journal of Polymer Research, 6*, 191–196. https://doi.org/10.1007/s10965-006-0087-y

Nicu, R., Lisa, G., Darie-Nita, R. N., Avadanei, M. I., Bargan, A., Rusu, D., & Ciolacu, D. E. (2024). Tailoring the structure and physico-chemical features of cellulose-based hydrogels using multi-epoxy crosslinking agents. *Gels, 10*, 523. https://doi.org/10.3390/gels10080523

Nouailhas, H., Aouf, C., Le Guerneve, C., Caillol, S., Boutevin, B., & Fulcrand, H. (2011). Synthesis and properties of biobased epoxy resins. Part 1. Glycidylation of flavonoids by epichlorohydrin. *Journal of Polymer Science Part A: Polymer Chemistry, 49*, 2261–2270. https://doi.org/10.1002/pola.24659

Obaid, A. O., Zbedy, A. S. A., Alrashdi, K. S., Aljohani, M. M., Alqarni, S. A., Al-Bonayan, A. M., Abumelha, H. M., & El-Metwaly, N. M. (2025). Mercury capture using functionalized metal-organic framework encapsulated in dual hydrogel layers of β-cyclodextrin and polyethylenimine: Synthesis, characterization, adsorption, thermodynamics, and Box-Behnken design analysis. *Carbohydrate Polymer Technologies and Applications*. , Article 100793. https://doi.org/10.1016/j.carpta.2025.100793

Oishi, K., & Maehata, Y. (2013). Removal properties of dissolved boron by glucomannan gel. *Chemosphere, 91*, 302–306. https://doi.org/10.1016/j.chemosphere.2012.11.034

Paufique, J., 2010. Cosmetic active ingredient, useful *e.g.* for the preparation of cosmetic composition to fight against the effects of skin aging and strengthen the facial and neck skin, comprises oligo-glucomannan derived from Amorphophallus konjac.

Pizzi, A. (2008). Chapter 8 - tannins: Major sources, properties and applications. In M. N. Belgacem, & A. Gandini (Eds.), *Monomers, polymers and composites from renewable resources* (pp. 179–199). Amsterdam: Elsevier. https://doi.org/10.1016/B978-0-08-045316-3.00008-9.

Postulkova, H., Chamradova, I., Pavlinak, D., Humpa, O., Jancar, J., & Vojtova, L. (2017). Study of effects and conditions on the solubility of natural polysaccharide gum karaya. *Food Hydrocolloids, 67*, 148–156. https://doi.org/10.1016/j.foodhyd.2017.01.011

Randhir, R., Lin, Y.-T., & Shetty, K. (2004). Stimulation of phenolics, antioxidant and antimicrobial activities in dark germinated mung bean sprouts in response to peptide and phytochemical elicitors. *Process Biochemistry, 39*, 637–646. https://doi.org/10.1016/S0032-9592(03)00197-3

Said, N. S., & Sarbon, N. M. (2022). Physical and mechanical characteristics of gelatin-based films as a potential food packaging material: A review. *Membranes, 12*, 442. https://doi.org/10.3390/membranes12050442

Sansonetti, A., Bertasa, M., Canevali, C., Rabbolini, A., Anzani, M., & Scalarone, D. (2020). A review in using agar gels for cleaning art surfaces. *Journal of Cultural Heritage, 44*, 285–296. https://doi.org/10.1016/j.culher.2020.01.008

Shavandi, A., Bekhit, A. E.-D. A., Saeedi, P., Izadifar, Z., Bekhit, A. A., & Khademhosseini, A. (2018). Polyphenol uses in biomaterials engineering. *Biomaterials, 167*, 91–106. https://doi.org/10.1016/j.biomaterials.2018.03.018

Shutava, T., Prouty, M., Kommireddy, D., & Lvov, Y. (2005). pH responsive decomposable layer-by-layer nanofilms and capsules on the basis of tannic acid. *Macromolecules, 38*, 2850–2858. https://doi.org/10.1021/ma047629x

Song, C., Lv, Y., Qian, K., Chen, Y., & Qian, X. (2019). Preparation of konjac glucomannan–borax hydrogels with good self-healing property and pH-responsive behavior. *Journal of Polymer Research, 26*, 52. https://doi.org/10.1007/s10965-019-1702-z

Spiridon, I., & Popa, V. I. (2008). Chapter 13 - hemicelluloses: Major sources, properties and applications. In M. N. Belgacem, & A. Gandini (Eds.), *Monomers, polymers and composites from renewable resources* (pp. 289–304). Amsterdam: Elsevier. https://doi.org/10.1016/B978-0-08-045316-3.00013-2.

Srzednicki, G., & Borompichaichartkul, C. (2020). *Konjac glucomannan: production, processing, and functional applications*. CRC Press.

Szabo, M., Idiţoiu, C., Chambre, D., & Lupea, A. (2007). Improved DPPH determination for antioxidant activity spectrophotometric assay. *Chemical Papers, 61*(3), 214–216. https://doi.org/10.2478/s11696-007-0022-7

Tang, Z., Chowdhury, I. F., Yang, J., Li, S., Mondal, A. K., & Wu, H. (2025). Recent advances in tannic acid-based gels: Design, properties, and applications. *Advances in Colloid and Interface Science, 339*, Article 103425. https://doi.org/10.1016/j.cis.2025.103425

Tang, Z., Yang, J., Li, S., Wu, Z., & Kanti Mondal, A. (2024). Anti-swellable, stretchable, self-healable, shape-memory and supramolecular conductive TA-based hydrogels for amphibious motion sensors. *European Polymer Journal, 211*, Article 113034. https://doi.org/10.1016/j.eurpolymj.2024.113034

Vera, M., & Urbano, B. F. (2021). Tannin polymerization: An overview. *Polymer Chemistry, 12*, 4272–4290. https://doi.org/10.1039/D1PY00542A

Vigani, B., Valentino, C., Sandri, G., Caramella, C. M., Ferrari, F., & Rossi, S. (2022). Spermidine crosslinked Gellan gum-based “Hydrogel nanofibers” as potential tool for the treatment of nervous tissue injuries: A formulation study. *IJN, 17*, 3421–3439. https://doi.org/10.2147/IJN.S368960

Villanueva, X., Zhen, L., Ares, J. N., Vackier, T., Lange, H., Crestini, C., & Steenackers, H. P. (2023). Effect of chemical modifications of tannins on their antimicrobial and antibiofilm effect against gram-negative and gram-positive bacteria. *Frontiers in Microbiology, 13*. https://doi.org/10.3389/fmicb.2022.987164

Wei, Q., Zhao, Y., Wei, Y., Wang, Y., Jin, Z., Ma, G., Jiang, Y., Zhang, W., & Hu, Z. (2023). Facile preparation of polyphenol-crosslinked chitosan-based hydrogels for cutaneous wound repair. *International Journal of Biological Macromolecules, 228*, 99–110. https://doi.org/10.1016/j.ijbiomac.2022.12.215

Zhang, W., Ren, X., Zhang, L., & Chen, J. (2022). Preparation and performance of thickened liquids for patients with Konjac Glucomannan-mediated dysphagia. *Molecules, 27*, 2194. https://doi.org/10.3390/molecules27072194

Zhen, L., Lange, H., & Crestini, C. (2021a). An analytical toolbox for fast and straightforward structural characterisation of commercially available tannins. *Molecules, 26*, 2532. https://doi.org/10.3390/molecules26092532

Zhen, L., Lange, H., Zongo, L., & Crestini, C. (2021b). Chemical derivatization of commercially available condensed and hydrolyzable tannins. *ACS Sustainable Chemistry & Engineering, 9*, 10154–10166. https://doi.org/10.1021/acssuschemeng.1c02114

Zhou, J., Li, M., Wu, J., Zhang, C., He, Z., Xiao, Y., Tong, G., & Zhu, X. (2022a). One-pot synthesis of hydroxyl terminated hyperbranched semi-aromatic poly(ester-imide)s. *Polymer, 253*, Article 124970. https://doi.org/10.1016/j.polymer.2022.124970

Zhou, N., Zheng, S., Xie, W., Cao, G., Wang, L., & Pang, J. (2022b). Konjac glucomannan: A review of structure, physicochemical properties, and wound dressing applications. *Journal of Applied Polymer Science, 139*, Article 51780. https://doi.org/10.1002/app.51780

Zhou, Z., Xiao, J., Guan, S., Geng, Z., Zhao, R., & Gao, B. (2022c). A hydrogen-bonded antibacterial curdlan-tannic acid hydrogel with an antioxidant and hemostatic function for wound healing. *Carbohydrate Polymers, 285*, Article 119235. https://doi.org/10.1016/j.carbpol.2022.119235